applied sciences

MDPI

Article

Audio Magnetotelluric and Gravity Investigation of the High-Heat-Generating Granites of Midyan Terrane, Northwest Saudi Arabia

Essam Aboud [1,*], Aref Lashin [2], Faisal Zaidi [3], Abdulaziz Al-Bassam [4], Nassir Al Arifi [3], Mohamed Abu Anbar [5] and Emad Al-Homadhi [2]

1 Geohazards Research Centre, King Abdulaziz University, Jeddah 21589, Saudi Arabia
2 Natural Gas Engineering Department, College of Engineering-Petroleum, King Saud University, Riyadh 11421, Saudi Arabia
3 Geophysics Department, College of Science-Geology, King Saud University, Riyadh 11451, Saudi Arabia
4 National Center for Water Research and Studies (NCWRS), Ministry of Environment, Water and Agriculture, Riyadh 11195, Saudi Arabia
5 Geology Department, Faculty of Science, Tanta University, Tanta 31527, Egypt
* Correspondence: eaboudishish@kau.edu.sa

Abstract: The Midyan Terrane (northwest Saudi Arabia) is characterized by the presence of a massive belt of radioactive granitic rocks and thick sedimentary cover near the coastal areas. The area is greatly influenced by the tectonic activities of the Red Sea and Gulf of Aqaba, implying its high potentiality of geothermal energy. In the present work, geophysical surveys, including audio magnetotelluric and gravity methods, were integrated to investigate the subsurface structural pattern of the study area, which identified regional deep and shallow fault systems and detected the subsurface geometry/extension of the granitic rocks as well as detecting the thickness of the sedimentary basins near the coastal area. A total number of 80 audio magnetotelluric and 246 gravity stations were recorded, analyzed, and interpreted. Two high-potential geothermal targets were indicated: high-heat-generating granites and thick anomalous sedimentary basins near the coastal areas. High-heat-generating granites are significant in terms of enhanced geothermal systems (EGSs) whereas sedimentary basins play a crucial role in the formation of conventional geothermal systems. Both areas require more exploration plans to evaluate the energy potential of geothermal reservoirs. The results also contribute to the identification of the subsurface orientation and geometry of radioactive granites, providing the necessary parameters to enhance a volumetric estimation for geothermal reserves.

Keywords: audio magnetotelluric; gravity; granite; Midyan Terrane; Saudi Arabia

Citation: Aboud, E.; Lashin, A.; Zaidi, F.; Al-Bassam, A.; Al Arifi, N.; Abu Anbar, M.; Al-Homadhi, E. Audio Magnetotelluric and Gravity Investigation of the High-Heat-Generating Granites of Midyan Terrane, Northwest Saudi Arabia. *Appl. Sci.* **2023**, *13*, 3429. https://doi.org/10.3390/app13063429

Academic Editors: Doug Arent, Xiaolei Yang and Adam Warren

Received: 1 January 2023
Revised: 14 February 2023
Accepted: 6 March 2023
Published: 8 March 2023

1. Introduction

Saudi Vision 2030 sets a target to transform from an oil-based economy to a diversified economy based on renewable and sustainable energy to offer a supply of 9.5 GW by 2030 [1]. Thus, the Saudi government introduced several initiatives for investment in renewable energy such as wind, solar, and geothermal [2–5]. Saudi Arabia has a series of hot springs (hydrothermal systems) and volcanic basaltic fields along the Red Sea coast that can be used for conventional geothermal systems. These resources are associated with tectonic (or volcanic) heating, which is related to the opening of the Red Sea/Gulf of Aqaba [6,7]. An excellent ridge of hot dry rock (e.g., high-heat-generating granites) is also recognized in the Arabian shield and northwestern parts, which can be considered to be hot dry rocks (HDRs) that are good for enhanced geothermal systems (EGSs).

EGSs, sometimes called hot dry rocks (HDRs), have been verified for 40 years [8]. The idea of an EGS is the use of hydraulic fracturing to create an artificial geothermal reservoir at deep depths (3–5 km). The technology of EGSs has been verified and is still under development all over the world. A total number of 18 sites of EGSs around the world (e.g., United States, Australia, the EU, South Korea, and Japan) are operating and under development [9]. The advantages of EGSs are that these technologies can function as baseload resources that produce power 24 h/day and they are available anywhere in the world. Good locations are over deep granite covered by a 3–5 km layer of insulating sediments that slow heat loss. An EGS plant is expected to have an economical lifetime of 20–30 years using current technology [10]. A global review of EGSs can be found in [9].

Worldwide, many authors have investigated geothermal resources, including EGSs, using a variety of geological, geochemical, and geophysical techniques in the last few years [11–14]. More specifically, geophysical methods such as gravity, electromagnetic, and magnetotelluric have been regionally applied to explore geothermal HDRs at different basins in the world such as the Cooper Basin, Australia, and the Gonghe Basin, China.

The geophysical resistivity method is one of the methods that can be used to explore and investigate geothermal resources. It provides information about the rock properties (e.g., porosity and permeability) and the degree of hydrothermal alteration, which can be used to determine the geometry and depths of geothermal reservoirs and to locate the fracture zones by means of resistivity contrasts [15,16]. The electrical resistivity of geothermal reservoir rocks is associated with porosity, water, and the exchange capacity, and is strongly controlled by temperature. Therefore, exploring low-resistivity areas by geophysical methods based upon electric resistivities plays a significant role in identifying high-temperature zones related to geothermal reservoirs [11,17].

One of the most important geophysical methods to map resistivity is the audio magnetotelluric (AMT) method. It is a natural source method that uses a frequency range from 1 Hz to 20 kHz (audio frequencies) and higher. It is commonly used in geothermal exploration. On the other hand, the gravity method, based on measuring the differences in the Earth's gravitational field at different locations, is usually used to understand the subsurface geological features on various scales [18]. The density models obtained from gravity data are non-unique solutions. However, gravity information can be successfully used in conjunction with AMT data by using integrated inversion procedures [19]. The final geological models represent the solution of a joint minimization process of both datasets.

Geophysical exploration methods have contributed to the development of geothermal energy in Australia. One of the first successful projects for the exploration of HDRs using geophysical techniques was that undertaken by Geodynamics Limited (GDY) in the Cooper Basin in South Australia [20]. The project site was selected where high-temperature granites were located at relatively shallower depths, as estimated by a temperature distribution map and a seismic reflection as well as the gravity survey results. An electromagnetic survey was conducted to evaluate the underground resistivity structure. A number of injections and production wells were drilled, tapping the geothermal reservoir. Water circulation through the reservoir was successfully conducted, and produced electricity of 1 MW in 2013.

He et al. [21] investigated geothermal HDRs in the Gonghe Basin, China, using gravity data to delineate a shallow underground fault and basement structure using a gravity analysis. Based on the interpretation of the gravity section inversion and Euler deconvolution, they concluded that the study area was in a high-heat-flow spot, and fitted well with the regional geological structure. A more recent study was performed by Zhao et al. [22] in the Gonghe Basin. They applied the 3D inversion method to satellite gravity data of the Gonghe Basin to analyze the underground structure and the mechanism of the geothermal system. They identified an internal heat source and a heat transfer channel, and concluded that crustal high-temperature partial molten mass was likely to be the main heat source for the hot dry rock geothermal resources in the Gonghe Basin.

In Saudi Arabia, EGSs are mainly encountered in the northwestern parts of the Midyan Terrane. A massive belt of high-heat granitic rocks that attains anomalously high-radioactive elements (U, Th, and K) are recognized [23]. It mainly consists of intrusive alkali, peralkaline granitic, and granodiorite rocks, along with a few extrusive rhyolites and dykes with high-radioactive magmatic sources. The heat-generation capacity of these granites varies from 2 to 134 μWm^{-3}. Merely 1 cubic meter of such granites can generate

10 MWe for 30 years. Assuming at least 2% of energy is extracted from such granites, on a conservative amount, 120×10^6 TWh electricity can be generated [24].

Generally, there is a big gap in the knowledge and information concerning the potential of geothermal resources in Saudi Arabia. During the last decade, a few studies have been made regarding the geothermal resources of Saudi Arabia; among them, [23–30] are the most important. Good work has been achieved by Aboud et al. [29], who built a database of the available geothermal resources in the kingdom and produced the first geothermal favorability map for the kingdom. However, more detailed and much more comprehensive exploration studies are required to evaluate the geothermal resources in Saudi Arabia, with a special emphasis on EGSs.

In this regard, audio magnetotelluric (AMT) and gravity geophysical measurements were obtained for a geothermal exploration of the Midyan area. The aims of this study were to investigate the subsurface structural pattern affecting the EGSs, describe the regional deep and shallow fault systems, characterize the thicknesses of the sedimentary cover, and detect the subsurface geometry/extension of the high-production granitic rocks; this will help to enhance detailed volumetric estimations, which are necessary for further geothermal reserve studies.

2. Geological Setting

The study area covered the whole of the Midyan Terrane in the northernmost part of Saudi Arabia (Figure 1). It extends from the Duba area at the southern part to the extreme northern part of the Al Bad' area. The area is exposed to a huge series of hard rocks, mainly meta-luminous, alkali, peralkaline granitic, and granodiorite rocks, and constitutes the north-western part of the Arabian–Nubian Shield, formed by the accretion of island arc terrain between 850 and 500 Ma [31,32]. These series are aligned along a northwest–southeast direction following the main trend of the Red Sea rift. The peralkaline granites (Midyan) constitute the last granitic phase of the Pan-African thermal event and the development of the Arabian Shield [33–35]. The area of interest also comprises sediments and rocks ranging in age from Quaternary to Precambrian. The Late Cretaceous to Tertiary deposits that exist in the study area are also well-exposed at the Midyan Peninsula, which fell within the study area [36].

Northwest–southeast-aligned granite mountains covered a wide part of the study area; however, thin stratigraphic units were recognized in the wides, represented mainly by Wadi fills and eroded materials. A seaward thickening towards the sedimentary cover is well-recognized, especially in the Neom area. Excepting the areas where granitic rocks were exposed, the lithological column of the area as detected from the few drilled shallow wells in the study area (MEWA, 2014) could be summarized as:

- Thin sedimentary cover, represented mainly by Wadi fills and eroded materials ranging in depth from 0 to 40 m in the valley's areas.
- Massive Precambrian granite rocks, from 40 m and decreasing.

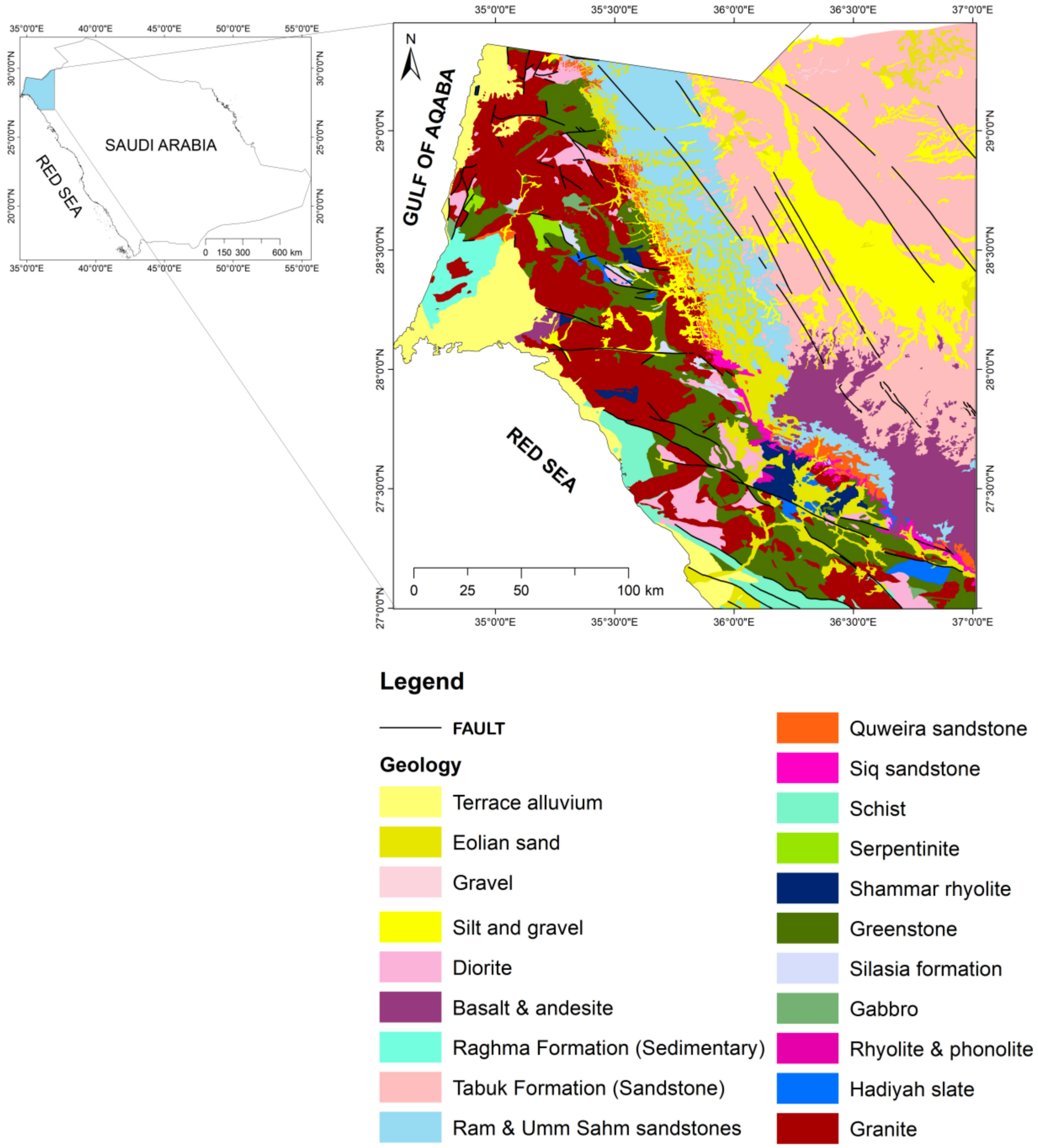

Figure 1. Geological map of Midyan Terrane showing the distribution of massive granites and other different rock units (after Faisal et al. [30]).

3. Material and Methods

AMT and gravity methods are commonly used in geothermal explorations where resistivity and density can be mapped, respectively. Resistivity and density play an important role in finding the permeability and porosity, which are directly associated with geothermal reservoirs [37–39].

In this study, first, the AMT method was utilized to image the subsurface resistivity structure. A KMS-820 instrument was used to record the AMT data. The data-acquisition system was developed for EM and seismic applications to obtain the subsurface resistivity and velocity, respectively. This method is commonly used in oil and gas exploration as well as geothermal studies. By using KMS-820 units, we collected AMT data at 80 stations.

Second, a gravity survey was utilized to delineate the subsurface structure in terms of the density variation. A special emphasis was given to the subsurface imaging of the extension of the granitic rocks that were exposed at the surface, forming a massive regional belt. A total number of 246 gravity stations were collected using a CG5 gravimeter. The gravity method has been successfully used to describe regional faults, fracture zones, and the thickness of sedimentary layers [37]. However, the ambiguity of gravity data is still an issue in all gravity surveys. It can be reduced by high-level overlap-acquired datasets.

After obtaining high-resolution data (e.g., relatively dense gravity stations), detailed density profiles could be utilized with the AMT data to perform a joint inversion. Figure 2 shows the locations of the AMT and gravity stations.

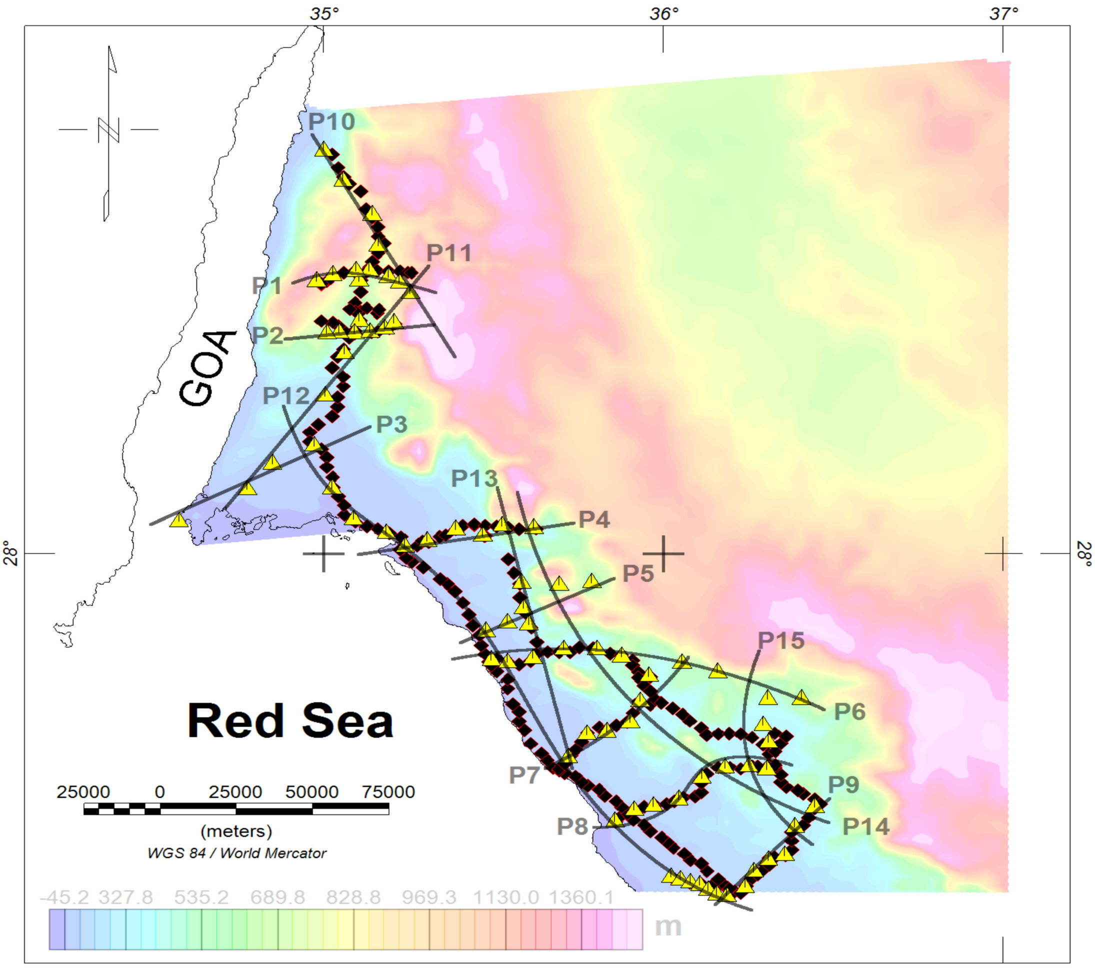

Figure 2. Yellow-filled triangles show the location of the AMT stations; black-filled red squares are the gravity stations. P1–P15 are the selected profiles for modelling; DEM is the background.

3.1. AMT Data

AMT data were acquired with a 3–5 km station interval. A KMS-820 recording system was used with 4 non-polarized electrodes (LEMI-701; Ag-AgCl + Pb-PbCl) and 2 high-frequency magnetic induction coils (LEMI-118; 1–70,000 Hz). The non-polarized electrodes were spread out on the ground at the recording site at a 50 m distance from the center in north–south and east–west directions. The recording unit and induction-coil magnetometers were located at the center in north–south and east–west directions (10 m away from the data logger). A total of 3 frequency bands were recorded at 80 kHz, 20 kHz, and 4 kHz for 3 min 57 s, 5 min 16 s, and 13 min 10 s, respectively.

By using the above configuration, the AMT data at 80 sites were measured during the fieldwork using the time-varying of natural electrical and magnetic fields. The relationship between the EM field components was represented in the frequency domain as a four-element impedance tensor. The AMT data were acquired in a passive mode using a combination of electrodes and induction-coil magnetometers. The electrodes were used to determine the electric field, which was derived from the measurements of the voltage difference between electrode pairs Ex and Ey. The induction coils were used to measure the magnetic field components (Hx and Hy) in orthogonal directions. The ratio of the recorded electric and magnetic fields in the frequency domain (Ex/Hy) provided an estimate of the apparent resistivity of the subsurface at depth.

The AMT data were recorded in a binary format, and then KMS pro software [40] was used to display, edit, filter, and sample the time series. Finally, a statistical means tool was used to estimate the impedance tensor from the spectra. The data were then ready to be imported into WinGLink software for the inversion [41].

The inversion algorithm strategy was based on analyzing the AMT data by the comparison of different geothermal benchmark modelling and inversion try-out results using a variety of inversion methods. Before that, the AMT stations were rotated by 45° to be a normal to regional geological strike (northwest). To image the subsurface resistivity structure in two dimensions, the AMT data were inverted using the algorithm of Rodi and Mackie [42] within the WinGLink software. This routine finds a regularized solution to the 2D inverse problem by using the non-linear conjugate gradients method [42].

3.2. Gravity Data

The gravity data were collected using a CG5 gravimeter with a ~2.5 km station interval. The gravity data were acquired along east–west profiles, which were almost at the same locations as the AMT, in order to detect fault systems below the surface and to facilitate the integration of both datasets in the interpretation.

The gravity data were processed by applying the most common corrections (e.g., tidal, instrument drift, latitude, free air, and Bouguer corrections). After removing the regional trend [43,44] from within the gravity data, the residual Bouguer anomaly map was displayed (Figure 3). It showed that the average anomaly values ranged from −60 to 42 mGal. Low- and high-gravity anomalies matched well with the surface geology.

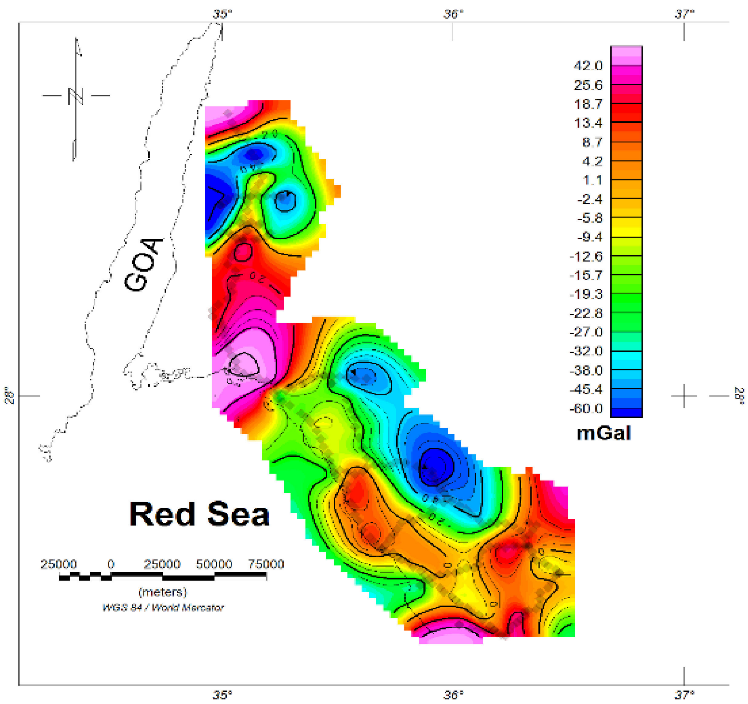

Figure 3. The Bouguer anomaly map of the study area. Dimmed squares show the location of the recorded gravity stations.

4. Results

4.1. AMT Data Analysis

The AMT data were analyzed to extract the subsurface structure and to determine the high-permeability fracture zones and up-flow zones of hydrothermal systems [15].

To image the subsurface resistivity structure in two dimensions, the AMT data were inverted [13,42]. In the inversion procedure, we used a smooth model inversion routine in which regularized solutions for the 2D inverse problem using a non-linear conjugate gradient could be obtained. The program inverted the 2D mesh, extending laterally and downward beyond the core region and incorporating the topography into the 2D mesh. The error floors were set to 5% for TE and TM (Rho and Phase). The inversion routine assumed that the profiles were perpendicular to the electrical strike (e.g., the geoelectric strike after rotation). Figures 4–6 show the 2D inversion results of a few selected profiles after 100 iterations. In the same figure, the results of gravity modelling for the same profiles are displayed.

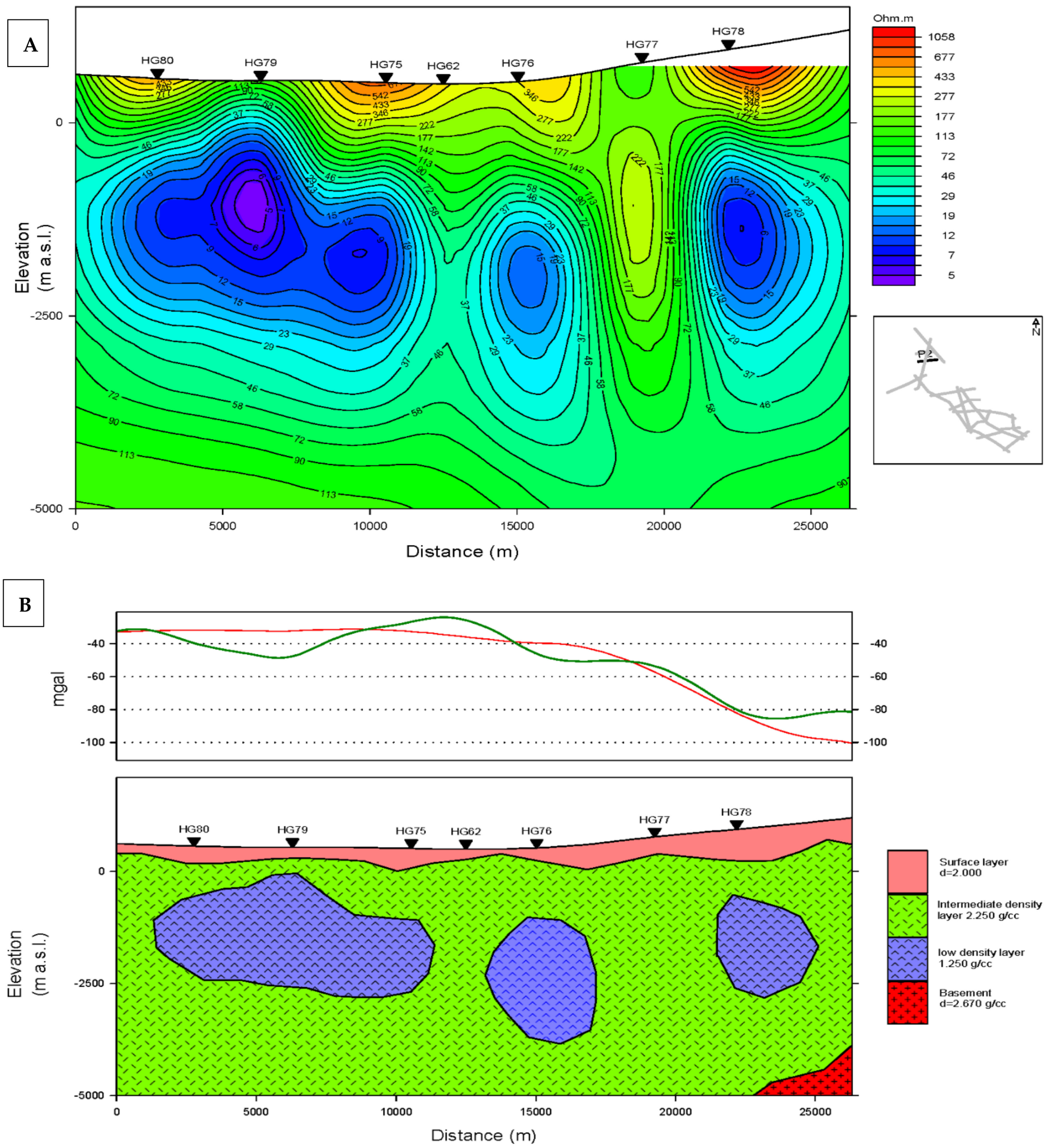

Figure 4. Profile-2 cross-section derived from (**A**) 2D modeling of AMT data (upper panel) and (**B**) density modelling (lower panel).

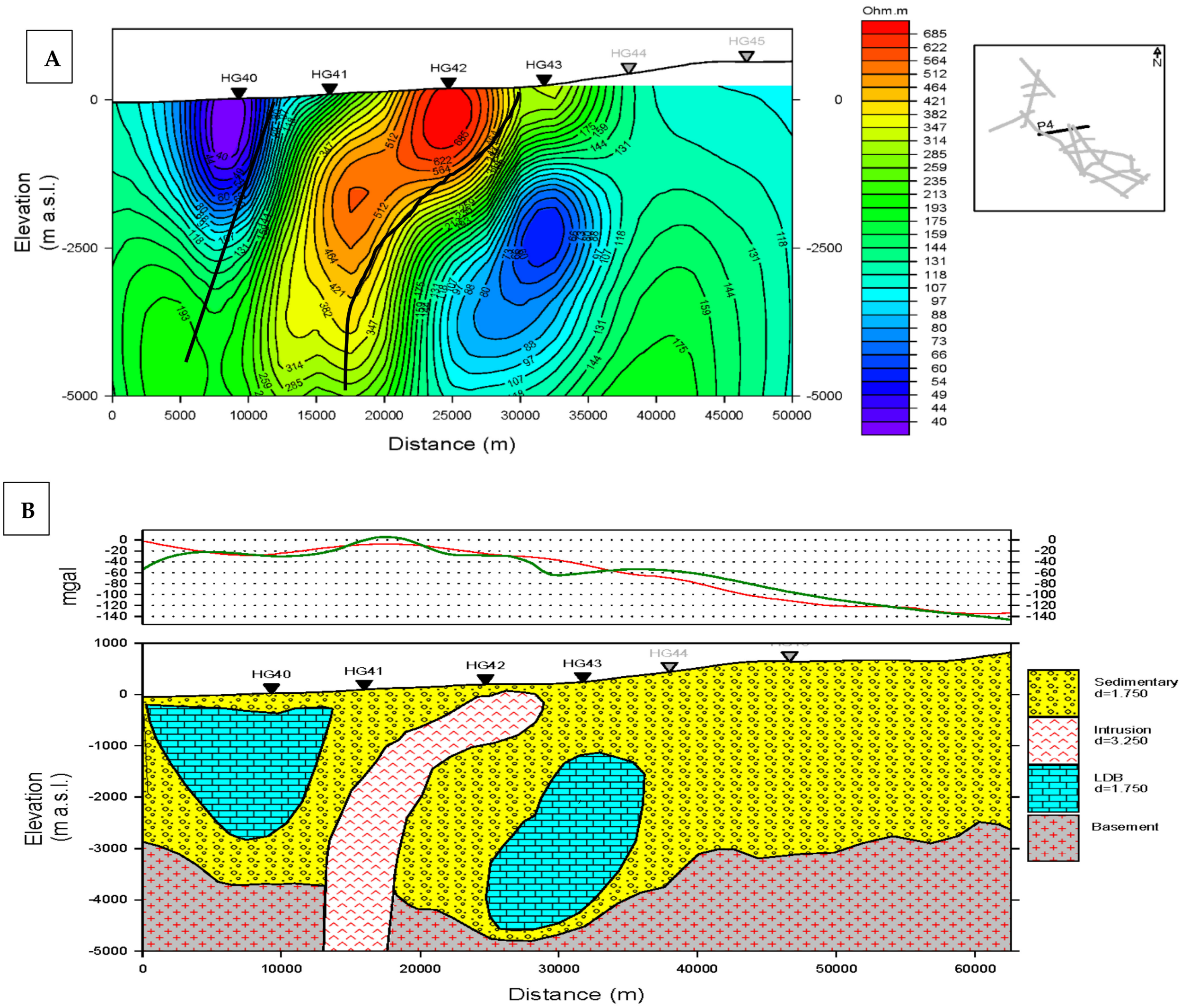

Figure 5. Profile-4 cross-sections derived from (**A**) 2D modeling of AMT data (upper panel) and (**B**) density modelling (lower panel).

4.2. Gravity Data Analysis

In a geothermal context, the optimal temperature for electricity generation is between 120–170 °C where the rock permeability is low [45]. In this case, it is important to characterize tectonic features such as faults and fractures that could act as permeable zones.

In this study, the subsurface density distribution beneath the Midyan region was predicted based on gravity data modelling. As no deep wells were drilled in the study area, the density models of the granite rocks were matched as much as possible with the available analyses of several exposed granite rocks in addition to the information provided from nearby drilled wells penetrating similar granitic rocks in the Arabian shield [46].

The resistivity curves and gravity modelling were overlapped for a clear interpretation. The inversion results of the AMT and gravity data were evaluated in terms of relatively low resistivity/density zones, which might have indicated a thermal variation. Accordingly, 15 profiles (Figure 2) were selected for inversion process (AMT and gravity).

4.3. Interpretations

Integrating the AMT and gravity data provided a more robust interpretation. The 2D inversion of the AMT data imaged the potential targets from the 2D resistivity inversions that were supported by the gravity-derived interpretations (e.g., low-density fracture/fault zones). The cross-sections showed the 2D-jointly interpreted AMT and gravity sections.

These sections were selected to demonstrate the different structural patterns and the geometry and extension of high-heat granites.

Figure 4 displays the 2D cross-section of Profile-2, extending along the east–west direction with a total length of 26 km. The section demonstrated the presence of low-resistivity subsurface anomalies (5–29 ohm.m), indicating a thick sedimentary cover (~3–3.5 km). On the other side, the 2D gravity model showed a similarity with the AMT section, and indicated that the relief of the basement was deeper towards the west.

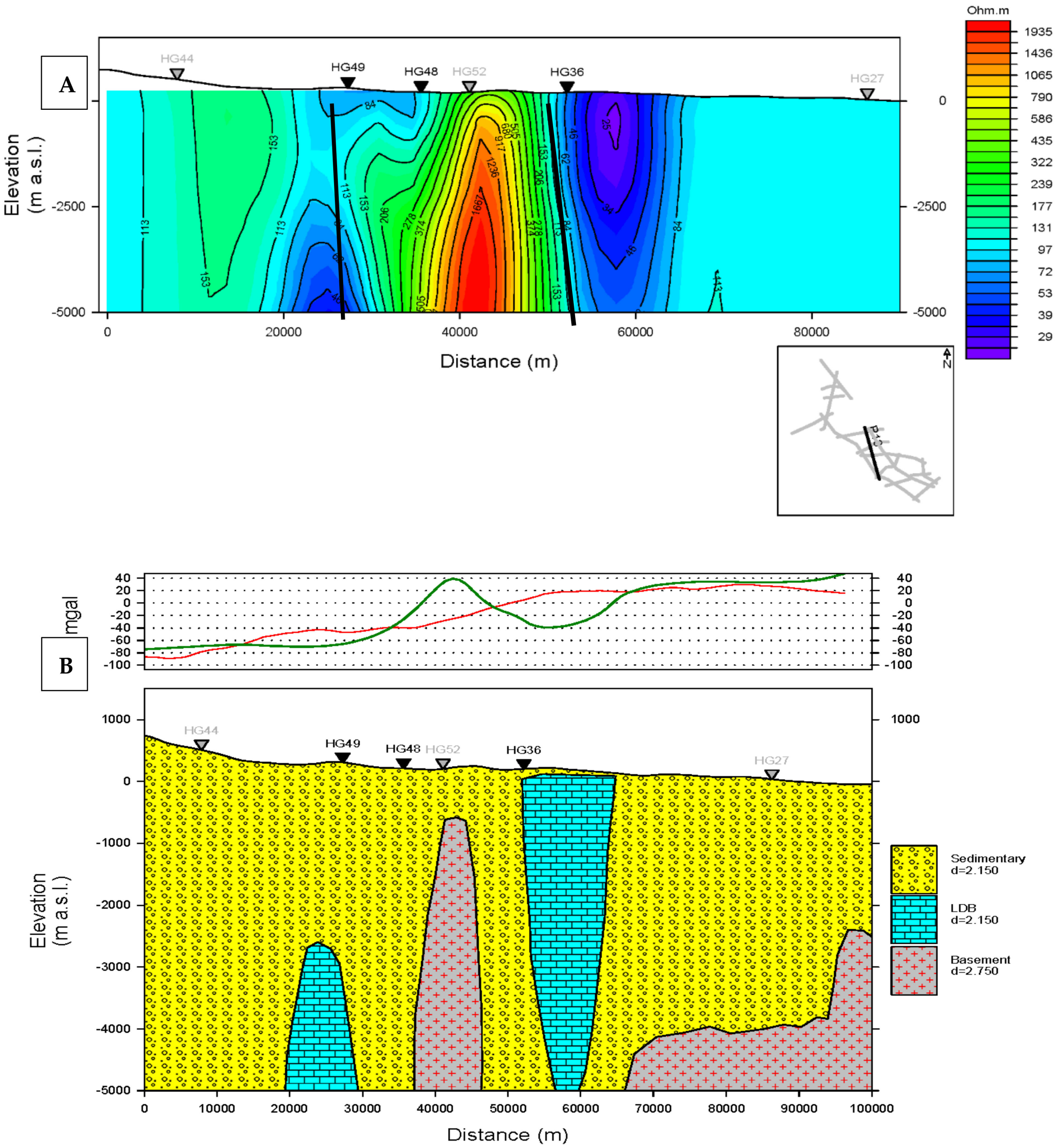

Figure 6. Profile-13 cross-sections derived from (**A**) 2D modeling of AMT data (upper panel) and (**B**) density modelling (lower panel).

Figure 5 shows the cross-section of Profile-4, extending 48 km in length and aligned along almost an east–west direction. The section showed a highly resistive region (347–685 ohm.m) sandwiched by two low-resistive anomalies (40–97 ohm.m). This region was associated with granitic rocks and bounded by faults parallel to the Red Sea (shown by black lines in Figure 5). The 2D gravity model also showed a high-density massive granitic rock in the middle of the modeled density section. The basement rocks appeared with an irregular relief at a depth of around 3000 m, with its main massive body extending downward (>5000 m).

Figure 6 shows the cross-section of Profile-13, extending north–south with a total length of 92 km. It shows a highly oriented resistive area (790–1935 ohm.m) associated with an intrusion of granitic rock into the sedimentary layer. Two east–west faults bounded this massive granitic body. These faults most probably belonged to the east–west transform faults that are common in the Arabian Shield. The gravity model showed that the basement was shallow to the south (right side) and deep to the north (left side). The high-density massive granitic body and its nearby low-density low-resistivity rocks was indicated well in the middle of the modeled density section.

5. Discussion

The gravity and AMT data were jointly interpreted to delineate the subsurface structure, and image the extension and geometry of the granitic rocks. From the inversion results of the AMT data, resistivity maps at various depths (1, 1.5, 2.5, 3.0, 3.5, and 4.0 km) were extracted from 2D resistivity models, as shown in Figure 7.

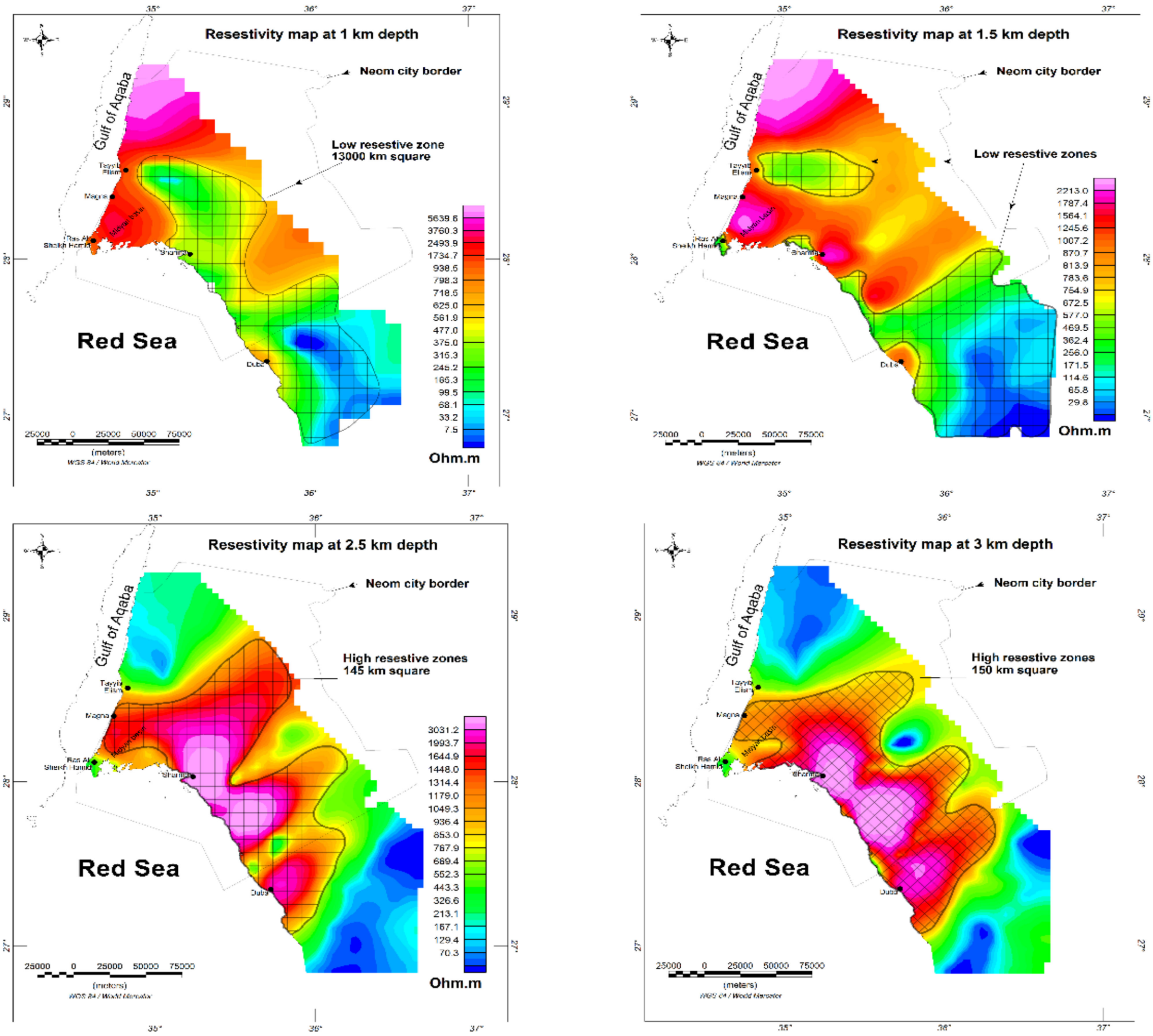

Figure 7. *Cont.*

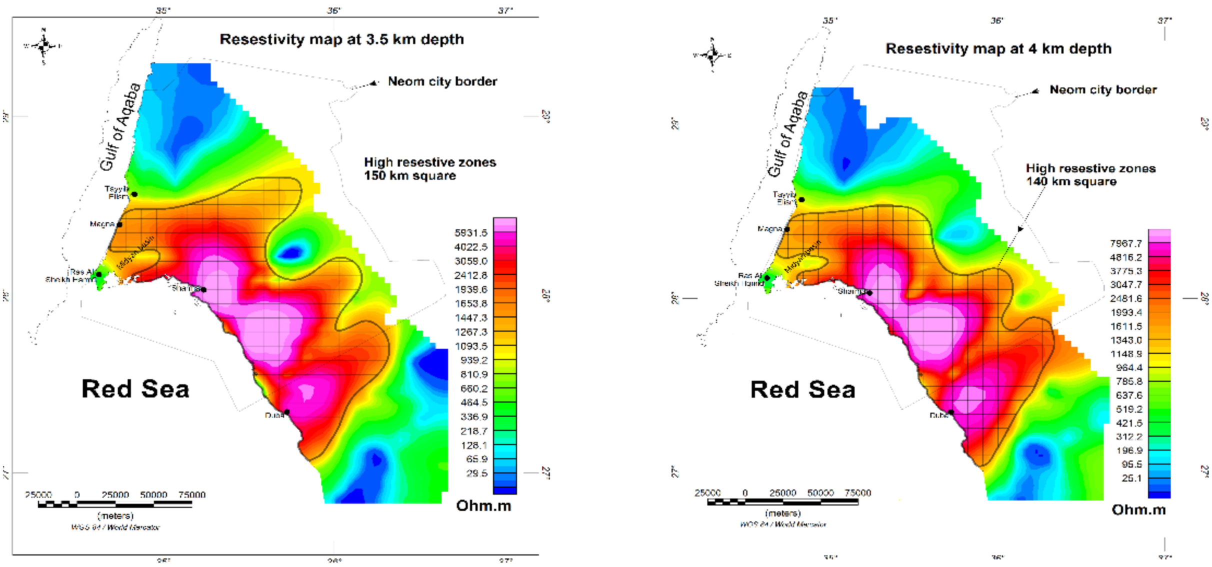

Figure 7. Extracted resistivity maps from AMT data inversion at various depths.

In a geothermal context, the study area had two potential targets. The first was the high-heat granites, which were well-delineated and mapped beneath the study area using the geophysical methods; namely, the AMT and gravity methods. The second was the thick sedimentary sections, which were mainly detected near the coastal parts of the study area. These could act as hot sedimentary aquifers.

The resistivity maps presented in Figure 7 show that the granitic rocks exhibited a good lateral and vertical extension, especially in the central and western parts of the study area. By estimating the volume of these granitic rocks within the optimal range of the cut-off temperature, a good reserve estimate could be executed. Assuming a cut-off grade temperature of 150 °C, these granitic rocks could be used for possible energy production. Chandrasekharam et al. [28] calculated the possible energy production.

The presence of good fracture and fault systems as well as medium-resistivity weathered granitic rocks is a key factor in selecting the best locations for drilling wells (exploration, injection, and production), which might suggest a full exploitation program of these geothermal resources. An appropriate energy transfer medium such as supercritical CO_2 can be injected into the fracture system of EGSs for possible energy production. However, more detailed geomechanical measurements are required to understand the mechanical properties of these granites.

Two important areas were deduced from the data analysis; i.e., areas with low resistive values (e.g., the blue polygons in Figure 8) and areas of high resistive values (the red crossed lines in Figure 8). Areas with low resistivity were considered to be hot sedimentary aquifers whereas areas with high resistive values represented the extension of high-heat granitic rocks.

The thicknesses of the sedimentary layers in these two areas were matched with the seismic reflection data of Tubbs et al. [47], who concluded that a temperature of 150 °C could be reached at a depth of 2500 m in the near-shore sections. Considering the thick sedimentary section (up to 3000 m) and assuming the temperature regime provided by [47], this area could be suggested as a good geothermal target (hydrothermal system).

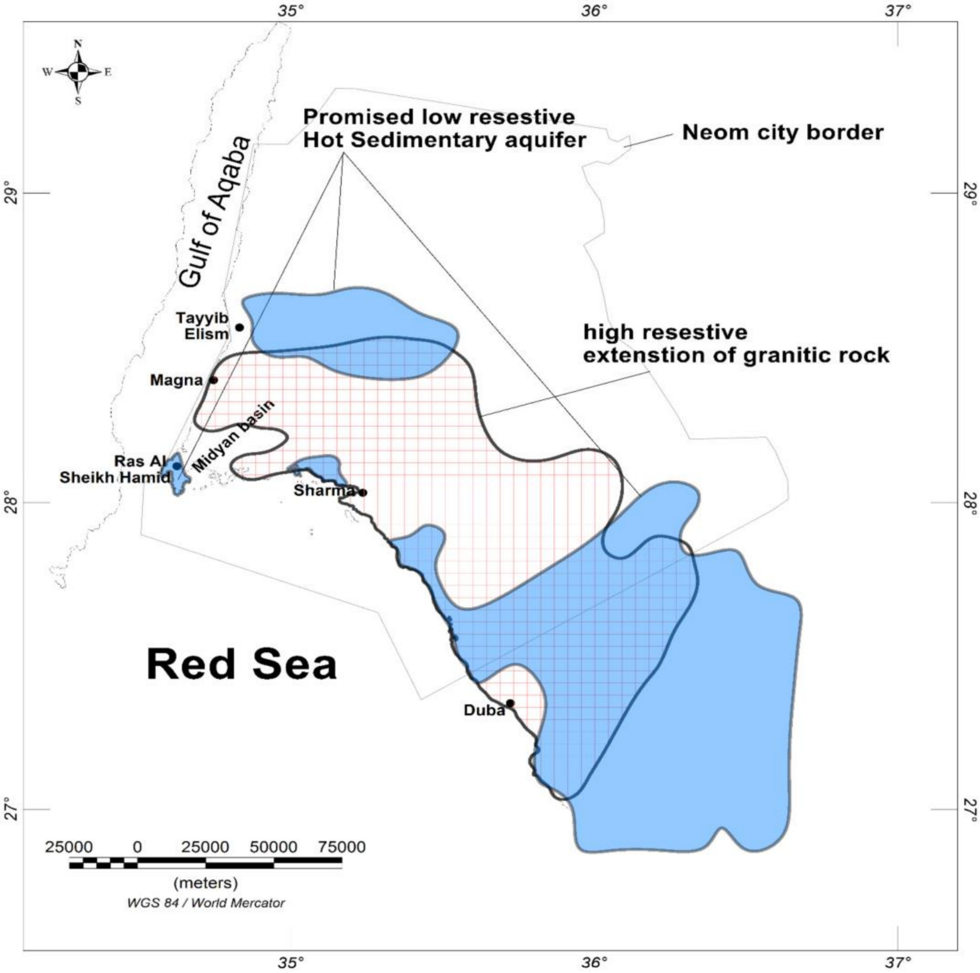

Figure 8. Final interpretation map showing the most promised zones (blue-filled polygons) for hot sedimentary basins and high-heat granitic rocks (red crossed grid).

6. Conclusions

- This study aimed to investigate high-production granitic rocks in the Midyan Terrane (northwest Saudi Arabia) through a joint analysis of audio magnetotelluric (AMT) and gravity data. A total number of 80 AMT and 246 gravity stations were measured, analyzed, and interpreted. A special emphasis was given to detect the subsurface structural patterns, detect the thicknesses of the sedimentary cover, identify regional deep and shallow fault systems, and clarify the subsurface geometry/extension of the granitic rocks. The main concluded points of this study can be summarized as follows:
- Geophysical AMT and gravity methods were successfully used to image the subsurface structure of the granitic rocks in the study area. These contributed more to the identification of the subsurface orientation and geometry of these granites, and provided the necessary parameters to enhance the further volumetric analysis of the geothermal potential.
- The area had a good geothermal potentiality, represented mainly by high-radioactive granites (EGS) and hot sedimentary basins.
- High-heat granite can be utilized as a good EGS source for possible energy production upon injecting an energy transfer medium such as CO_2 (supercritical CO_2). However, more detailed geomechanical measurements are required to understand the mechanical behaviors of these granites.
- Near-shore thick sedimentary basins, with a temperature up to 150 °C, are a good candidate for conventional geothermal energy (hydrothermal system). Two important

geothermal areas were indicated and mapped; thick sedimentary basins and high-heat granitic rocks.
- Both areas require more exploration activity in order to evaluate the geothermal energy reservoir and estimate its reserves.

Author Contributions: All authors contributed to the literature review, methodology, formal analysis, data interpretation, and writing and reviewing of the manuscript. All authors have read and agreed to the published version of the manuscript.

Funding: This research was funded by the National Plan for Science, Technology and Innovation (MAARIFAH), King Abdulaziz City for Science and Technology, Kingdom of Saudi Arabia, Award Number 14-ENE704-02.

Institutional Review Board Statement: Not applicable.

Informed Consent Statement: Not applicable.

Data Availability Statement: Not applicable.

Acknowledgments: The authors are grateful to the anonymous reviewers who helped in enhancing the manuscript.

Conflicts of Interest: The authors declare that the research was conducted in the absence of any commercial conflict of interest or financial relationships that could be construed as a potential conflict of interest.

References

1. Amran, Y.A.; Alyousef, R.; Alabduljabbar, H. Renewable and sustainable energy production in Saudi Arabia according to Saudi Vision 2030; Current status and future prospects. *J. Clean. Prod.* **2020**, *247*, 119602. [CrossRef]
2. Tlili, I. Renewable energy in Saudi Arabia: Current status and future potentials. *Environ. Dev. Sustain.* **2015**, *17*, 859–886. [CrossRef]
3. AlYahya, S.; Irfan, M.A. The techno-economic potential of Saudi Arabia's solar industry. *Renew. Sustain. Energy Rev.* **2016**, *55*, 697–702. [CrossRef]
4. Mosly, I.; Makki, A.A. Current Status and Willingness to Adopt Renewable Energy Technologies in Saudi Arabia. *Sustainability* **2018**, *10*, 4269. [CrossRef]
5. Al Yousif, A. Renewable energy challenges and opportunities in the Kingdom of Saudi Arabia. *Int. J. Econ. Financ.* **2020**, *12*, 1–10. [CrossRef]
6. Aboulela, H.; Amin, A.; Lashin, A.; El Rayes, A. Contribution of geothermal resources to the future of renewable energy in Egypt: A case study, Gulf of Suez-Egypt. *Renew. Energy* **2021**, *167*, 248–265. [CrossRef]
7. Boulos, F. Some aspects of the geophysical regime of Egypt in relation to heat flow, ground water and microearthquakes. In *The Geology of Egypt*; Said, R., Ed.; Routledge: Abingdon, UK, 1990; Chapter 6; pp. 61–89.
8. Duchane, D.; Brown, D. *Hot Dry Rock (HDR) Geothermal Energy Research and Development at Fenton Hill*; GHC Bulletin: Los Alamos, NM, USA, 2002; pp. 13–19.
9. Shyi-Min, L. A global review of enhanced geothermal system (EGS). *Renew. Sustain. Energy Rev.* **2018**, *81*, 2902–2921.
10. Tester, J.W.; Anderson, B.J.; Batchelor, A.S.; Blackwell, D.D.; Di Pippo, R.; Drake, E.M.; Garnish, J.; Livesay, B.; Moore, M.C.; Nichols, K. *The Future of Geothermal Energy—Impact of Enhanced Geothermal Systems (EGS) on the United States in the 21st Century*; Idaho National Laboratory: Idaho Falls, ID, USA, 2006; ISBN 0-615-13438-6.
11. Tschirhart, V.; Colpron, M.; Craven, J.; Ghalati, F.H.; Enkin, R.J.; Grasby, S.E. Geothermal Exploration in the Burwash Landing Region, Canada, Using Three-Dimensional Inversion of Passive Electromagnetic Data. *Remote Sens.* **2022**, *14*, 5963. [CrossRef]
12. Zhu, J.; Jin, S.; Yang, Y.; Zhang, T. Geothermal Resource Exploration in Magmatic Rock Areas Using a Comprehensive Geophysical Method. *Geofluids* **2022**, *2022*, 5929324. [CrossRef]
13. Saibi, H.; Khosravi, S.; Cherkose, B.A.; Smirnov, M.; Kebede, Y.; Fowler, A. Magnetotelluric data analysis using 2D inversion: A case study from Al- Mubazzarah Geothermal Area (AMGA), Al-Ain, United Arab Emirates. *Heliyon* **2021**, *7*, e07440. [CrossRef]
14. Guerrero, F.J.; Giovanni, S.C.; Rosa, M.P. A numerical model for the magmatic heat reservoir of the Las Tres Virgenes volcanic complex, Baja California Sur, Mexico. *J. Volcanol. Geotherm. Res.* **2021**, *414*, 107–227. [CrossRef]
15. Malin, P.E.; Onach, S.A.; Shalev, E. *A Collaborative Cooperative Constrained Geophysical Imaging Project at Krafla and IDDP: ICEKAP*; Duke University: Durham, NC, USA, 2004; pp. 12–26.
16. Zucchi, M. Faults controlling geothermal fluid flow in low permeability rock volumes: An example from the exhumed geothermal system of eastern Elba Island (northern Tyrrhenian Sea, Italy). *Geothermics* **2020**, *85*, 101765. [CrossRef]
17. Hacıoğlu, Ö.; Başokur, A.T.; Diner, Ç. Geothermal potential of the eastern end of the Gediz basin, western Anatolia, Turkey revealed by three-dimensional inversion of magnetotelluric data. *Geothermics* **2021**, *91*, 102040. [CrossRef]
18. Roy, K.K. *Potential Theory in Applied Geophysics*; Springer: Berlin/Heidelberg, Germany, 2008; 671p.

19. Árnason, K.; Eysteinsson, H.; Hersir, G.P. Joint 1D inversion of TEM and MT data and 3D inversion of MT data in the Hengill area, SW Iceland. *Geothermics* **2010**, *39*, 13–34. [CrossRef]
20. Kaieda, H.; Suzuki, S. Geophysical exploration for Hot Dry Rock geothermal energy development at Cooper Basin, Australia. *Butsuri Transa* **2014**, *67*, 277–285.
21. He, R.; Zeng, Z.; Zhao, X.; Du, W.; Huo, Z.; Song, E. Interpretation of gravity data to delineate underground structure in the Gonghe geothermal field, China. In Proceedings of the International Geophysical Conference, Qingdao, China, 17–20 April 2017; pp. 1–4.
22. Zhao, J.; Zeng, Z.; Zhou, S.; Yan, J.; An, B. 3-D Inversion of Gravity Data of the Central and Eastern Gonghe Basin for Geothermal Exploration. *Energies* **2023**, *16*, 2277. [CrossRef]
23. Hussein, M.T.; Lashin, A.; Al Bassam, A.; Al Arifi, N.; Al Zahrani, I. Geothermal power potential at the western coastal part of Saudi Arabia. Renew. Sustain. *Energy Rev.* **2013**, *26*, 668–684. [CrossRef]
24. Chandrasekharam, D.; Lashin, A.; Al Arifi, N. Meeting future energy demand of Saudi Arabia through high heat generating granites. *Int. J. Earth Sci. Eng.* **2014**, *7*, 1–4.
25. Lashin, A.; Al Arifi, N. Geothermal energy potential of southwestern of Saudi Arabia "exploration and possible power generation": A case study at Al Khouba area—Jizan. *Renew. Sustain. Energy Rev.* **2014**, *30*, 771–789. [CrossRef]
26. Lashin, A.; Pipan, M.; Al Arifi, N.; Al Bassam, A. Geophysical exploration of the western Saudi Arabian geothermal province: First results from the Al-Lith area. In Proceedings of the World Geothermal Congress, Melbourne, Australia, 19–25 April 2015; pp. 1–9.
27. Lashin, A.; Chandrasekharam, D.; Al Bassam, A.; Al Arifi, N.; Rehman, S. A review of the Geothermal Resources of Saudi Arabia: 2015–2020. In Proceedings of the World Geothermal Congress, Melbourne, Australia, 19–25 April 2015; pp. 1–12.
28. Chandrasekharam, D.; Lashin, A.; Al Arifi, N.; Al Bassam, A.; El Alfy, M.; Ranjith, P.; Varun, C.; Singh, H. The potential of high heat generating granites as EGS source to generate power and reduce CO_2 emissions, western Arabian shield, Saudi Arabia. *J. Afr. Earth Sci.* **2016**, *112*, 213–233. [CrossRef]
29. Aboud, E.; Qaddah, A.; Harbi, H.; Alqahtani, F. Geothermal resources database in Saudi Arabia (GRDiSA): GIS model and geothermal favorability map. *Arab. J. Geosci.* **2021**, *14*, 112. [CrossRef]
30. Zaidi, F.K.; Lashin, A.; Aboud, E.; Al Arifi, N.; Al-Bassam, A.; Al-Homadhi, E.; Abu Anbar, M. Silica geothermometry and multi indices approach to characterize groundwater from Midyan region in North-western Saudi Arabia. *J. Afr. Earth Sci.* **2022**, *192*, 104557. [CrossRef]
31. Stern, R.J. ARC assembly and continental collision in the Neoproterozoic East African Orogen: Implications for the Consolidation of Gondwanaland. *Annu. Rev. Earth Planet. Sci.* **1994**, *22*, 319–351. [CrossRef]
32. Stern, R.J.; Johnson, P. Continental lithosphere of the Arabian Plate: A geologic, petrologic, and geophysical synthesis. *Earth-Sci. Rev.* **2010**, *101*, 29–67. [CrossRef]
33. Radain, A.A.M.; Fyfe, W.S.; Kerrich, R. Origin of peralkaline granites of Saudi Arabia. *Contrib. Miner. Pet.* **1981**, *78*, 358–366. [CrossRef]
34. Stoeser, D.B.; Camp, E. Pan-African microplate accretion of the Arabian shield. *Geol. Soc. Am. Bull.* **1985**, *96*, 817–826. [CrossRef]
35. Alfotawi, B.; Gazzaz, M.; Hassan, M. Uranium and Thorium Enrichment in Haql Granite in Midyan Region Northwest of Saudi Arabia. *J. King Abdulaziz Univ. Sci.* **1991**, *4*, 161–170. [CrossRef]
36. Laboun, A.A. Did glaciers exist during Pleistocene in the Midyan region, northwest corner of the Arabian Peninsula? *Arab. J. Geosci.* **2012**, *5*, 1333–1339. [CrossRef]
37. Tulinius, H.; Ádám, L.; Halldórsdóttir, H.; Yu, G.; Strack, K.; Allegar, N.; He, L.F.; He, Z.X. Exploring for geothermal reservoirs using broadband 2-D MT and gravity in Hungary. In *SEG Technical Program Expanded Abstracts 2008*; Society of Exploration Geophysicists: Houston, TX, USA, 2008; pp. 1147–1151.
38. Daud, Y.; Sudarman, S.; Ushijima, K. Integrated geophysical studies of the Ulubelu geothermal filed, south Sumatera, Indonesia. In Proceedings of the World Geothermal Congress 2000, Kyushu-Tohoku, Japan, 28 May–10 June 2000.
39. Santos, P.A.; Rivas, J.A. *Gravity Surveys Contribution to Geothermal Exploration in El Salvador: The Cases of Berlin, Ahua Achapan and San Vicente Areas*; UNU-GTP-LaGeo: San Salvador, El Salvador, 2009; pp. 1–4.
40. KMS Technology. *KMS Pro Software, AMT Data Analysis Software*; KMS Technologies GmbH: Dresden, Germany, 2015.
41. *Schlumberger Software*; V. 2.21.08; WinGlink: A Geophysical Interpretation Software; Schlumberger: Houston, TX, USA, 2014.
42. Rodi, W.; Mackie, R.L. Nonlinear conjugate gradients algorithm for 2-D magnetotelluric inversions. *Geophysics* **2001**, *66*, 174–187. [CrossRef]
43. Gupta, V.K.; Ramani, N. Some aspects of regional residual separation of gravity anomalies in a Precambrian terrain. *Geophysics* **1980**, *45*, 1412–1426. [CrossRef]
44. Hammer, S. Deep gravity interpretation by stripping. *Geophysics* **1963**, *28*, 369–378. [CrossRef]
45. Gitonga, G. Geothermal power plants for medium and high temperature steam and an overview of wellhead power plants. In *Short Course II on Exploration and Development of Geothermal Resources*; UNU-GTP and KenGen: Naivasha, Kenya, 2018; pp. 1–7.
46. MEWA. Study of groundwater natural radioactive contamination phenomena. *Geophys. Well Logs Inf.* **2014**, *10*, 19–20.
47. Tubbs, R.E., Jr.; Fouda, G.A.H.; Afifi, A.M.; Raterman, N.S.; Hughes, G.W.; Fadolalkarem, Y.K. Midyan Peninsula, northern Red Sea, Saudi Arabia: Seismic imaging and regional interpretation. *GeoArabia* **2014**, *19*, 165–184. [CrossRef]